small methods

Supporting Information

for *Small Methods,* DOI: 10.1002/smtd.201900529

Highlighting the Reversible Manganese Electroactivity in Na-Rich Manganese Hexacyanoferrate Material for Li- and Na-Ion Storage

Angelo Mullaliu, Jakob Asenbauer, Giuliana Aquilanti, Stefano Passerini, and Marco Giorgetti**

Highlighting the Reversible Manganese Electroactivity in Na-rich Manganese Hexacyanoferrate Material for Li- and Na-ion Storage

Angelo Mullaliu [a,b], Jakob Asenbauer [a,b], Giuliana Aquilanti [c], Stefano Passerini [a,b]*, Marco Giorgetti [d]*

[a] Helmholtz Institute Ulm (HIU), Helmholtzstrasse 11, 89081, Ulm, Germany

[b] Karlsruhe Institute of Technology (KIT), P.O. Box 3640, 76021, Karlsruhe, Germany

[c] Elettra Sincrotrone Trieste, ss 14, km 163.5, 34149 Trieste, Basovizza, Italy

[d] Department of Industrial Chemistry "Toso Montanari", University of Bologna, Viale Risorgimento 4, 40136 Bologna, Italy

* Corresponding authors. Email. stefano.passerini@kit.edu; marco.giorgetti@unibo.it

Experimental set-up for the synthesis of Na-rich MnHCF

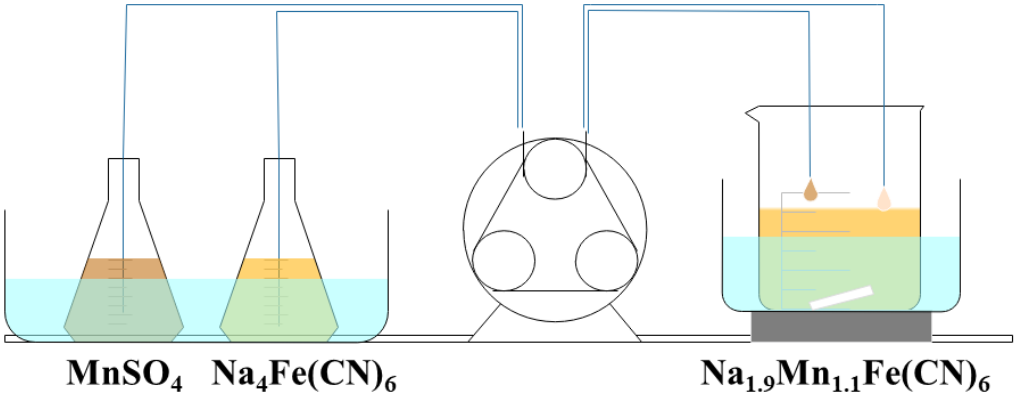

Figure S1. Sketch illustrating the experimental set-up adopted for the synthesis of Na-rich MnHCF.

Material characterization

TG analysis evidences a double-step loss of water molecules in the first 200°C (cf. Figure S2). The first loss occurs at relatively low temperature, while the second step is centered at 171.2°C (cf. inset Figure S2 and Table S1). As reported in the literature[16,32,33], PBAs often display a double-step loss of water, the first ascribable to adsorbed H_2O, the second to interstitial H_2O. We can, therefore, deduce that the amount of interstitial water in the hydrated compound corresponds to 8.6% of the total weight. Mass losses of minor entities are observed at roughly 350°C and 450°C, evidencing good thermal stability of the material at high temperatures.

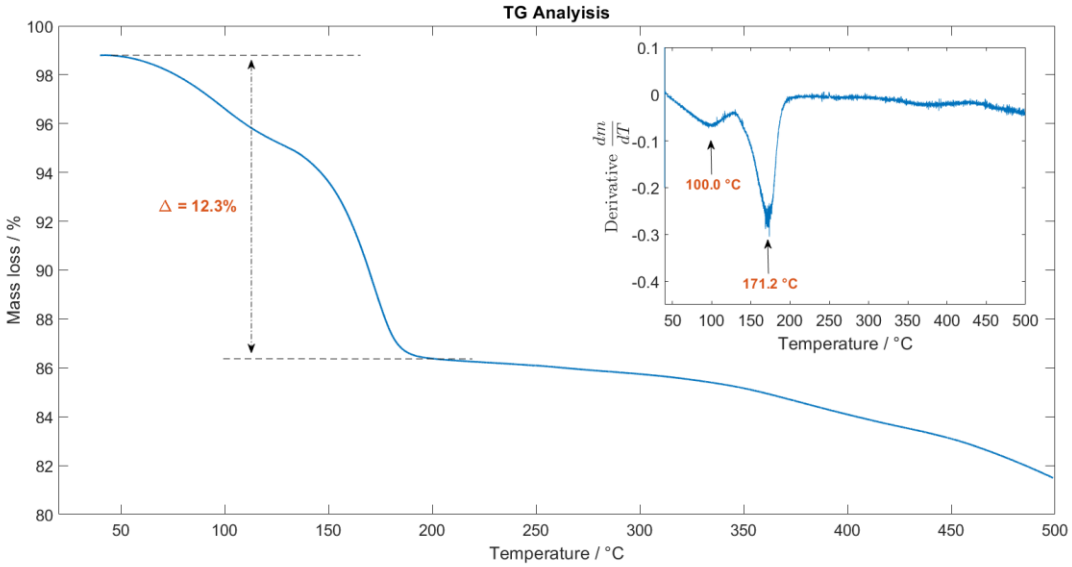

Figure S2. TGA curve recorded for the Na-rich MnHCF powder before vacuum-drying. The inset illustrates the derivative curve of the mass loss with respect to the temperature.

Table S1. Mass losses and respective temperature ranges from TG analysis.

	First step	**Second step**
Initial T loss / °C	40.0	129.0
Max T loss / °C	100.0	171.2
Final T loss / °C	129.0	199.0
ΔT range / °C	89.0	70.0
Mass loss / %	3.7	8.6

As retrieved from ICP measurements, the Na/Mn/Fe ratios is equal to 1.9/1.1/1.0 leading to the assumption that the considered compound presents a 10% of ferrocyanide ($[Fe(CN)_6]^{4-}$) vacancies.

Moreover, due to the high content of sodium per unit formula, the obtained compound can be assumed as sodium-rich. Overall, the material stoichiometry can be written as $Na_{1.9}Mn_{1.1}[Fe(CN)_6]$ $2.1H_2O$.

Table S2. Details on Na-rich MnHCF powder refinement: lattice parameters, fit goodness, and atomic positions.

Space group	$P2_1/n$
Symmetry operations	x, y, z x, -y, -z -x+1/2, y+1/2, - z+1/2 x+1/2, -y+1/2, z+1/2
a / Å	10.562 ± 0.005
b / Å	7.534 ± 0.004
c / Å	7.356 ± 0.004
β / deg	92.01 ± 0.04
Cell volume / Å^3	584.9_9
Rwp	14.2
χ^2	9.49

	Coordinates			
Atom label	**X**	**Y**	**Z**	**Wyckoff site position**

Mn1	0.5 (fixed)	0.5 (fixed)	0.5 (fixed)	2a
Fe1	0.5 (fixed)	0.0 (fixed)	0.0 (fixed)	2d
N1	0.503 ± 0.004	0.312 ± 0.008	0.753 ± 0.005	4e
N2	0.304 ± 0.004	0.487 ± 0.007	0.489 ± 0.005	4e
N3	0.511 ± 0.006	0.264 ± 0.009	0.281 ± 0.006	4e
C1	0.500 ± 0.006	0.186 ± 0.012	0.808 ± 0.008	4e
C2	0.184 ± 0.004	0.502 ± 0.006	0.480 ± 0.004	4e
C3	0.523 ± 0.008	0.189 ± 0.010	0.206 ± 0.007	4e
O1	0.253 ± 0.002	0.216 ± 0.003	0.280 ± 0.003	4e
Na1	0.25 ± 0.04	0.46 ± 0.06	0.014 ± 0.004	4e

Ex situ electrodes

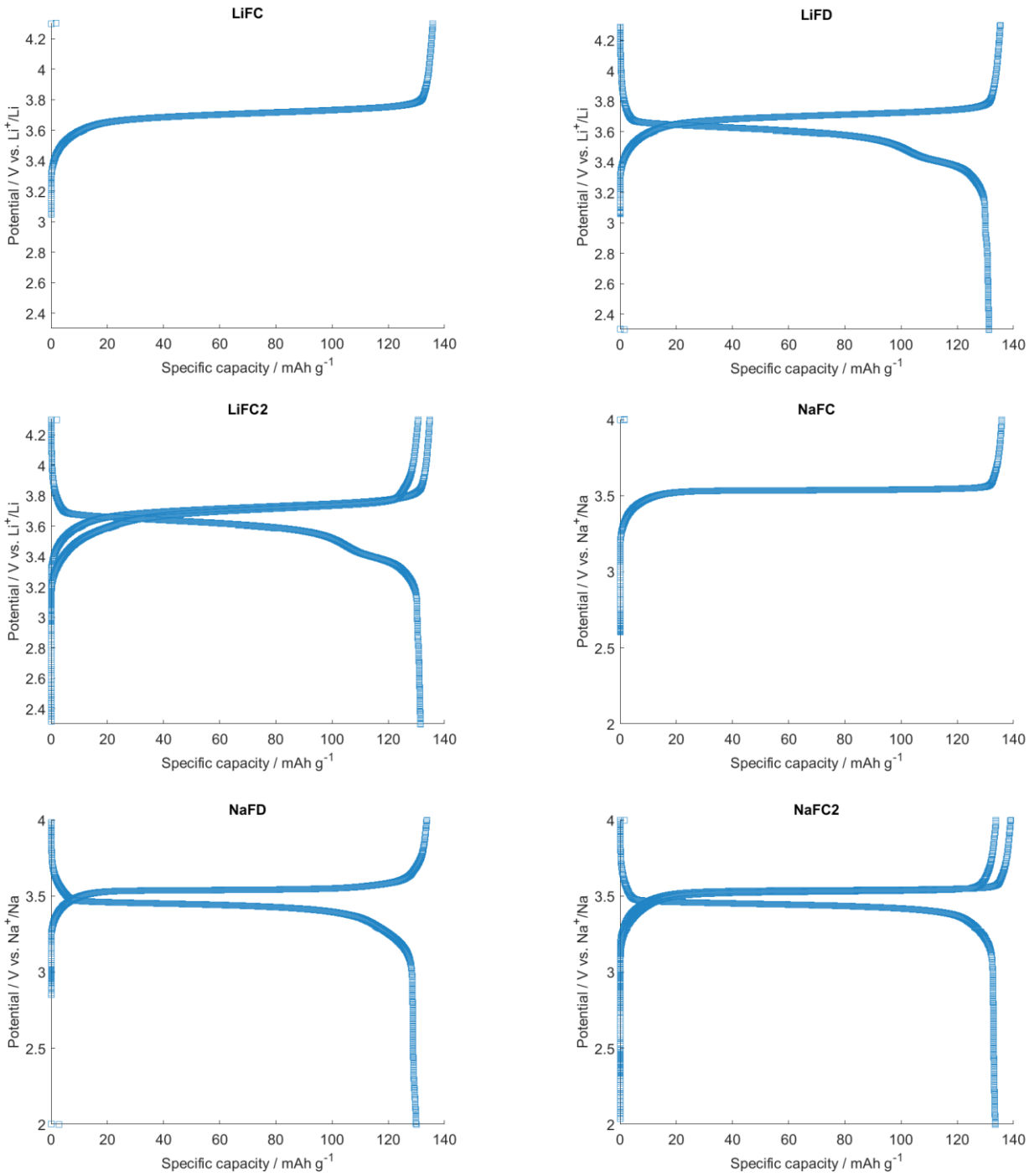

Figure S3. Electrochemical curves for all ex situ electrodes.

Pre-edge analysis

Pre-edge peaks analysis was carried out through the Peak analyzer tool of OriginPro 9 software. The baseline was obtained by fitting a polynomial function in the 6530-6550 eV range. Only two peaks and their centroid positions were considered, even though more transitions contribute to the peak shape. In particular, fully charged samples, i.e., LiFC, LiFC2, NaFC, and NaFC2, display a large peak width for the peak centered at 6546 eV (peak B), symptom of the occurrence of at least two transitions at this energy, likely due to the transitions to the 4p (as for discharged and pristine samples) and $d_{x^2-y^2}$ orbitals. Indeed, $d_{x^2-y^2}$ and the other 3d orbitals (d_{xy}, d_{xz}, d_{yz}, d_{z^2}) are well separated in energy after JT-elongation (as reported in Ref. [18]), occurring in concomitance with the oxidation of Mn^{2+} to Mn^{3+}.

Table S3. Mn pre-peak analysis on ex situ samples.

Sample	Peak A / eV	Peak B / eV
Pristine	6540.52	6546.07
LiFC	6540.45	6546.95
LiFD	6540.39	6546.07
LiFC2	6540.45	6546.65
NaFC	6540.45	6546.81
NaFD	6540.43	6546.07
NaFC2	6540.45	6546.65

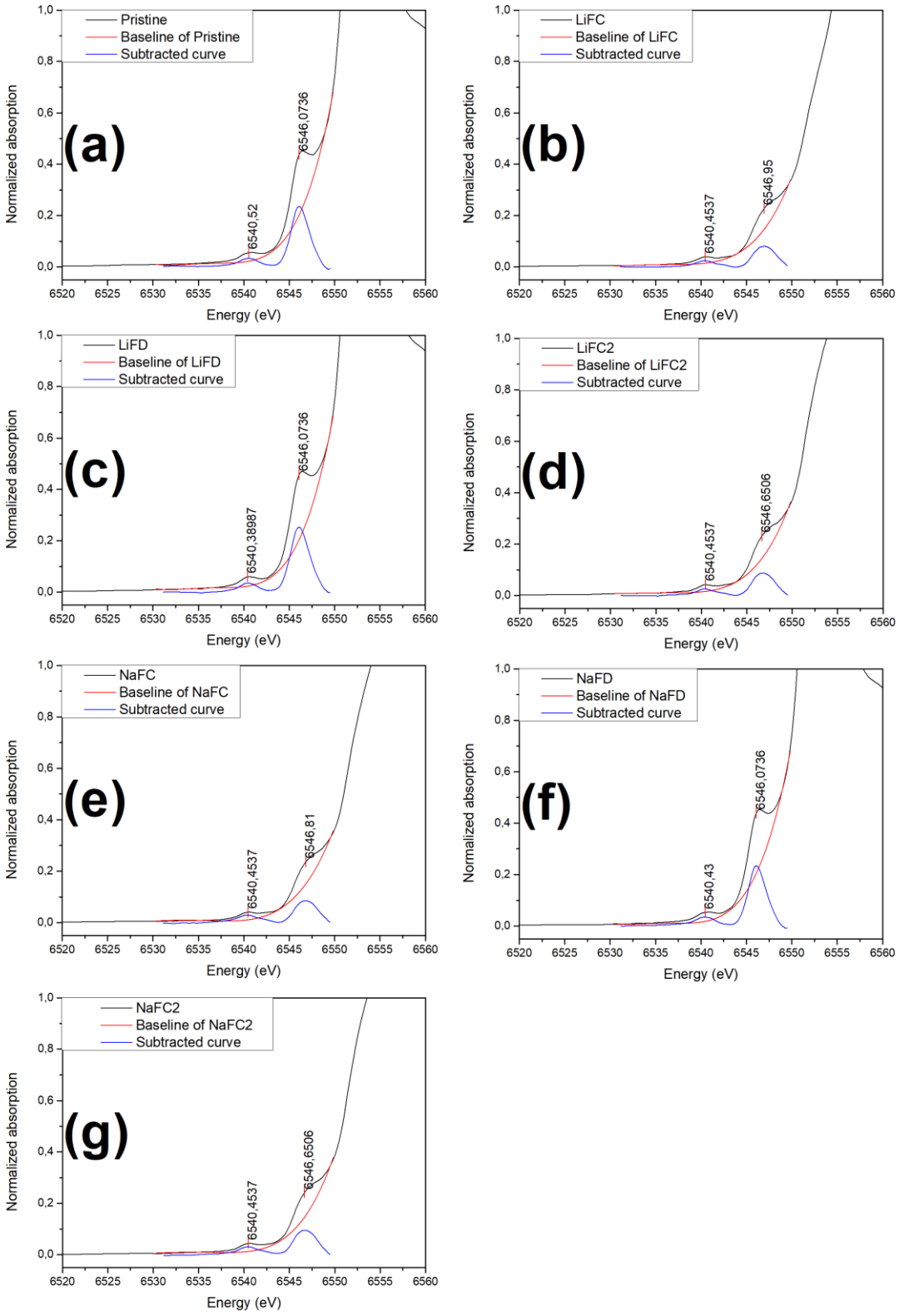

Figure S4. Pre-edge analysis on ex situ samples. **(a)** Pristine; **(b)** LiFC; **(c)** LiFD; **(d)** LiFC2; **(e)** NaFC; **(f)** NaFD; **(g)** NaFC2.

EXAFS analysis

Due to the extended Mn-NC-Fe network, both C≡N and Fe-C bond lengths are affected by the Mn JT-effect: in the charged states, Fe-C lengthens shortly, while CN shortens by a small extent. Bond lengths are completely restored to initial values in the reduced state.

In the preliminary EXAFS data analysis, asymmetric Mn-N_6 octahedra were considered for all states of charge, i.e., two Mn-N distances corresponding to Mn-N_{axial} and Mn-$N_{equatorial}$ were retrieved. As presented in **Table S4**, Mn-N distances in the reduced states (LiFD and NaFD) assume close values whose average is about 2.18 Å. Contrarily, the Mn-N_6 asymmetry, hence distortion, is enhanced in the oxidized states, where evaluated Mn-N_{axial} and Mn-$N_{equatorial}$ distances differ by 10%. To minimize the number of refinable parameters, two structural models were considered for reduced and oxidized states, adopting a symmetric Mn-N shell for the former and an asymmetric Mn site environment for the latter.

Table S4. EXAFS preliminary data treatment. Two Mn-N distances were considered for all states of charge.

	LiFD	**NaFD**	**LiFC**	**LiFC2**	**NaFC**	**NaFC2**
Mn-N_{axial} / Å	2.21	2.18	2.24	2.23	2.24	2.25
Mn-$N_{equatorial}$ / Å	2.16	2.17	2.01	1.99	2.00	2.00

Table S5. EXAFS fitting results.

	Pristine	**LiFD**	**NaFD**	**LiFC**	**LiFC2**	**NaFC**	**NaFC2**
Fe-C / Å	1.876(5)	1.876(5)	1.875(4)	1.901(3)	1.906(2)	1.902(2)	1.906(2)
σ^2 Fe-C / Å^2	0.003(1)	0.0033(6)	0.0031(4)	0.0023(4)	0.0022(4)	0.0025(4)	0.0021(3)
C≡N / Å	1.183(4)	1.181(4)	1.183(4)	1.162(5)	1.161(4)	1.162(3)	1.161(4)
σ^2 C≡N / Å^2	0.010(4)	0.010(2)	0.008(1)	0.0084(7)	0.0075(7)	0.011(2)	0.007(1)
Mn-N / Å	2.18(1)*	2.177(8)*	2.182(9)*	1.954(6)**	1.960(8)**	1.96(1)**	1.960(8)**
σ^2 Mn-N / Å^2	0.0065(15)	0.0066	0.0072	0.007(2)	0.008(2)	0.006(2)	0.008(2)
Mn-N / Å				2.19(2)***	2.22(2)***	2.22(2)***	2.22(2)***
σ^2 Mn-N / Å^2				0.017(7)	0.009(4)	0.009(4)	0.009(4)
σ^2 Fe-C-N / deg^2	45(20)	43(25)	45(20)	30(8)	30(8)	25(7)	30(9)
σ^2 Mn-N-C / deg^2	5(4)	7(5)	4(3)	7(6)	8(7)	15(8)	8(7)
θ Fe-C-N / deg	175	175	175	180	180	180	180
θ Mn-N-C / deg	FIX	FIX	FIX	FIX	FIX	FIX	FIX
E0 Mn	6541(1)	6542(1)	6541(1)	6544(1)	6544(1)	6545(1)	6544(1)
E0 Fe	7118.3(6)	7117.4(4)	7117.4(5)	7118(1)	7118(1)	7118(1)	7118(1)
S02 Fe	0.65(3)	fix	fix	fix	fix	Fix	Fix
S02 Co	0.81(3)	fix	fix	fix	fix	Fix	Fix
a/2 / Å							
χ^2-like residual / (10^{-6})	3.79	3.91	4.61	2.11	2.65	2.33	2.16

*CN =6. **CN=4. ***CN=2

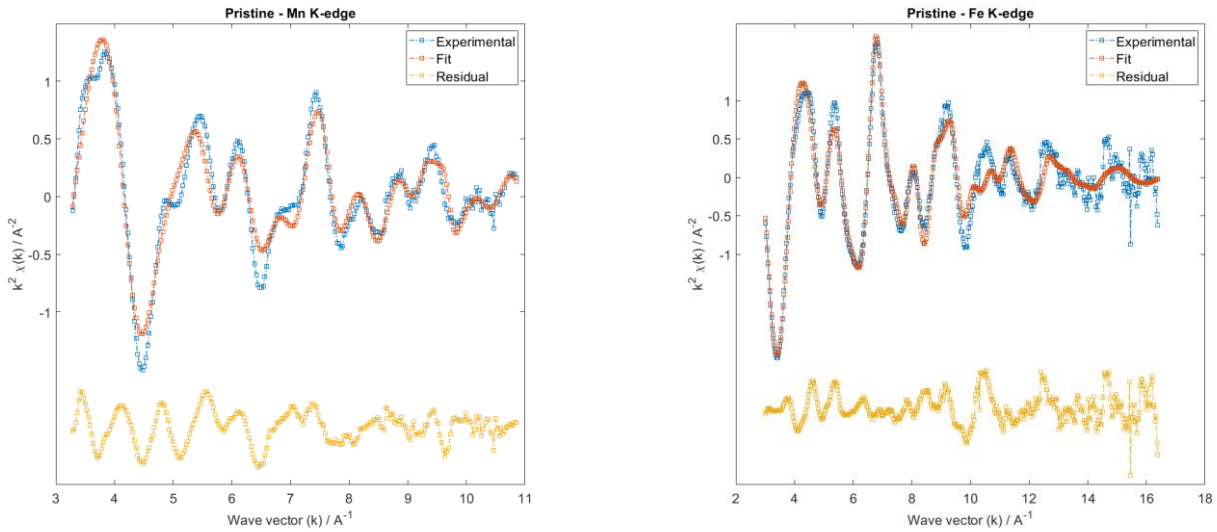

Figure S5. Comparison between experimental and theoretical EXAFS signals at the Mn and Fe K-edges for pristine state.

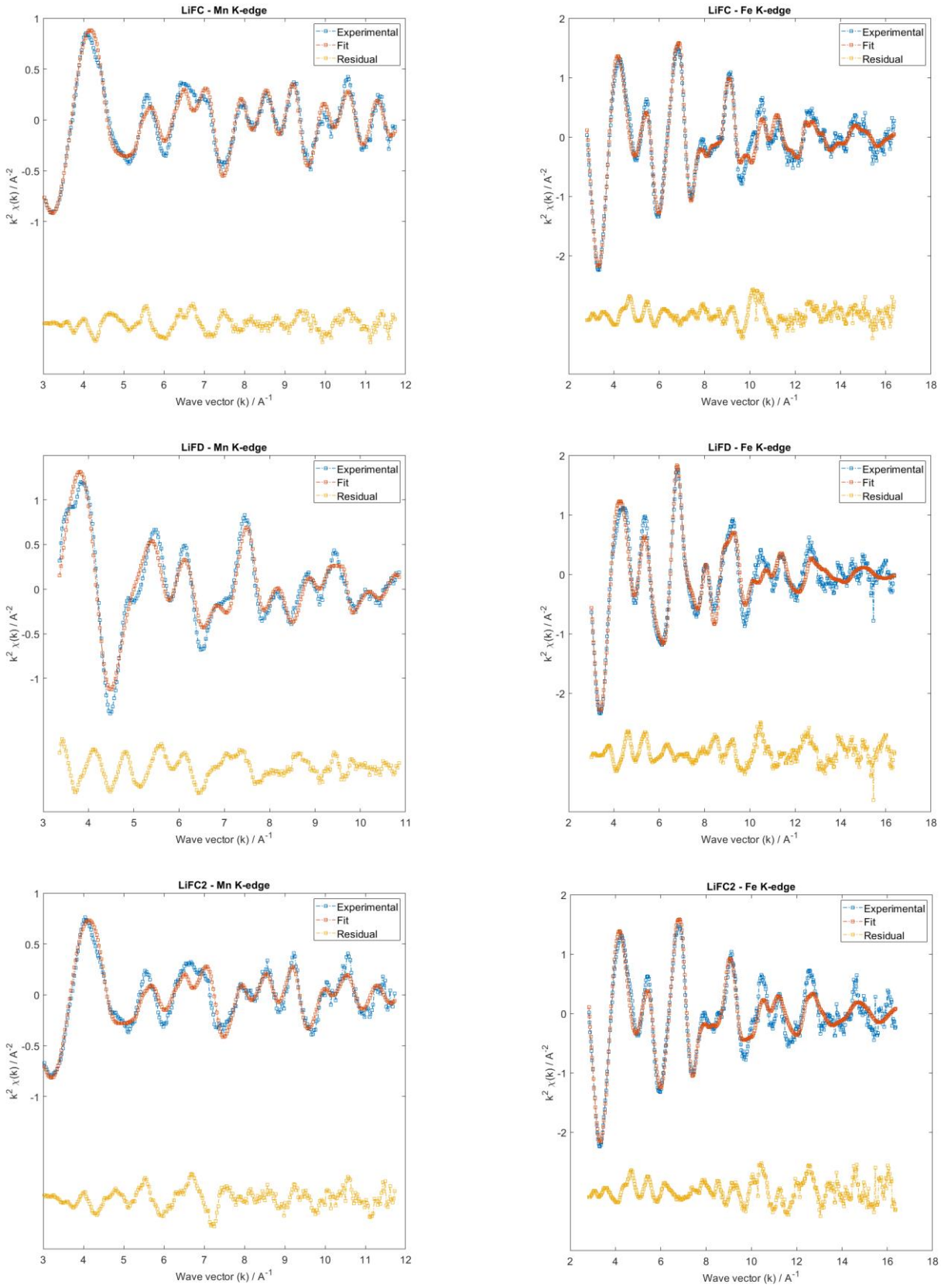

Figure S6. Comparison between experimental and theoretical EXAFS signals at the Mn and Fe K-edges for LiFC, LiFD, and LiFC2.

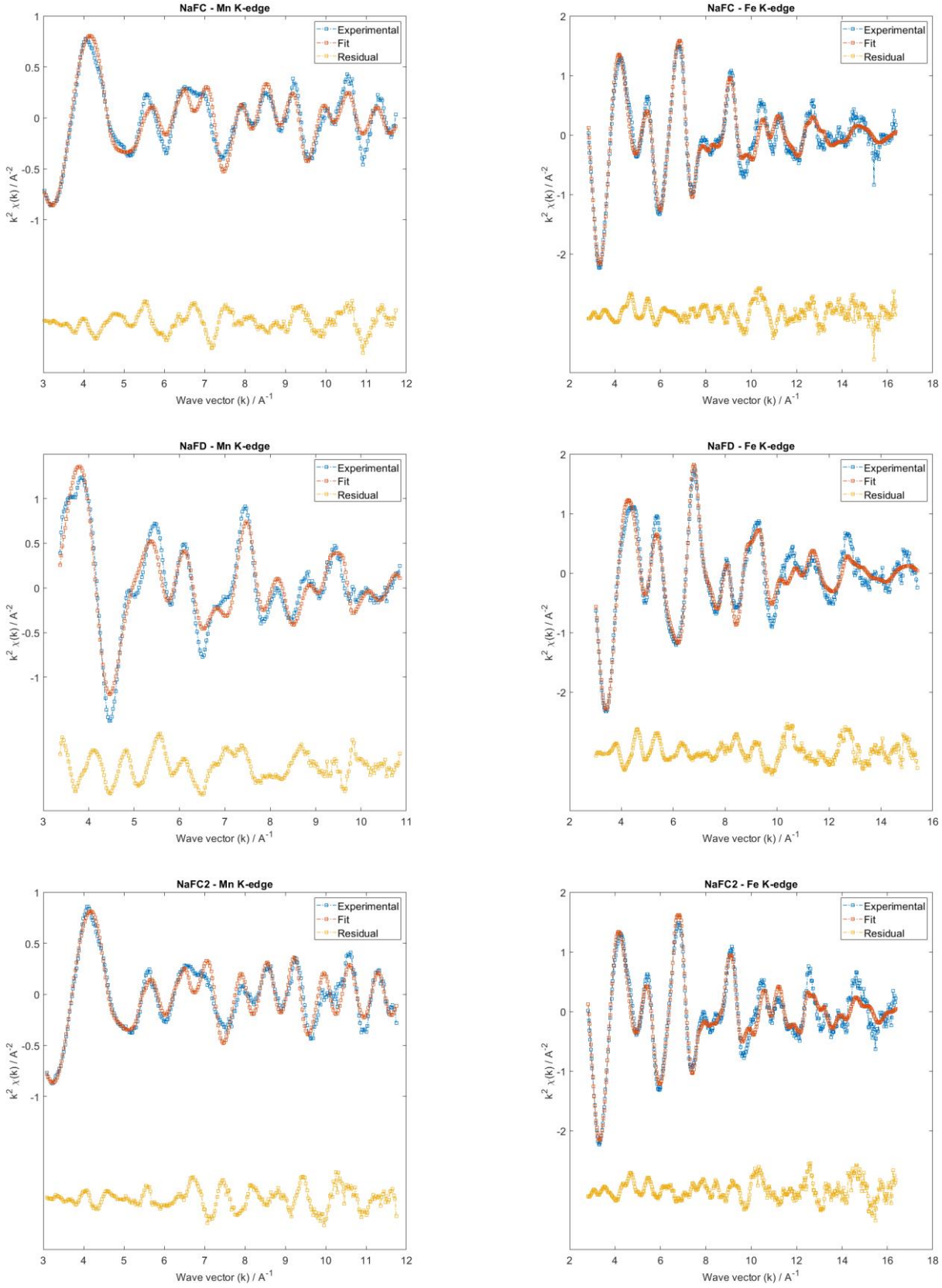

Figure S7. Comparison between experimental and theoretical EXAFS signals at the Mn and Fe K-edges for NaFC, NaFD, and NaFC2.